applied mechanics

Article

Resilient and Sustainable Structures through EMI-Based SHM Evaluation of an Innovative C-FRP Rope Strengthening Technique

Nikos A. Papadopoulos *, Maria C. Naoum, George M. Sapidis and Constantin E. Chalioris

Laboratory of Reinforced Concrete and Seismic Design of Structures, Civil Engineering Department, School of Engineering, Democritus University of Thrace, 67100 Xanthi, Greece; mnaoum@civil.duth.gr (M.C.N.); gsapidis@civil.duth.gr (G.M.S.); chaliori@civil.duth.gr (C.E.C.)
* Correspondence: nikpapad@civil.duth.gr

Abstract: Reinforced Concrete (RC) members in existing RC structures are susceptible to shear-critical due to their under-reinforced design. Thus, implementing a retrofitting technique is essential to eliminate the casualties that could arise from sudden and catastrophic collapses due to these members' brittleness. Among other proposed techniques, using Carbon-Fiber Reinforced Polymers (C-FRP) ropes to increase the shear strength of RC structural elements has proved to be a promising reinforcement application. Moreover, an Electro-Mechanical Impedance (EMI-based) method using Lead Zirconate Titanate (PZT-enabled) was employed to assess the efficiency of the strengthening scheme. Initially, the proposed technique was applied to C-FRP rope under the subjection of pullout testing. Thus, a correlation of the rope's tensile strength with the EMI responses of the PZT patch was achieved using the Root Mean Square Deviation (RMSD) metric index. Thereafter, the method was implemented to the experimentally acquired data of C-FRP ropes, used as shear reinforcement in a rectangular deep beam. The ropes were installed using the Embedded Through Section (ETS) scheme. Furthermore, an approach to evaluate the residual shear-bearing capacity based on the EMI responses acquired by being embedded in and bonded to the ropes' PZTs was attempted, demonstrating promising results and good precision compared to the analytical prediction of the C-FRP ropes' shear resistance contribution.

Keywords: structural health monitoring (SHM); electromechanical impedance (EMI); piezoelectric transducer (PZT); C-FRP rope; shear retrofitting technique; pullout

check for updates

Citation: Papadopoulos, N.A.; Naoum, M.C.; Sapidis, G.M.; Chalioris, C.E. Resilient and Sustainable Structures through EMI-Based SHM Evaluation of an Innovative C-FRP Rope Strengthening Technique. *Appl. Mech.* **2024**, *5*, 405–419. https://doi.org/10.3390/applmech5030024

Received: 28 April 2024
Revised: 30 May 2024
Accepted: 5 June 2024
Published: 21 June 2024

Copyright: © 2024 by the authors. Licensee MDPI, Basel, Switzerland. This article is an open access article distributed under the terms and conditions of the Creative Commons Attribution (CC BY) license (https://creativecommons.org/licenses/by/4.0/).

1. Introduction

A significant portion of reinforced concrete (RC) members within existing RC structures often suffer from under-reinforcement against shear, primarily due to obsolete and inadequate design provisions. These members are vulnerable to shear-critical cracking, posing the risk of brittle failures due to their insufficient strength capacity and deformation ability [1,2]. As a result, implementing retrofit techniques to bolster the shear bearing capacity becomes imperative to mitigate the potential casualties stemming from sudden and catastrophic collapses of these brittle RC members [3,4].

Among the array of available retrofitting techniques, RC jacketing is a popular choice for addressing deficiencies in RC members within existing structural sub-assemblages [5,6]. Numerous studies have highlighted the benefits of conventional RC jacketing in augmenting load-bearing capacity [7], stiffness, and overall structural response efficiency [8,9].

However, despite its efficacy, conventional RC jacketing has limitations. Challenges such as alterations in the structural dynamic characteristics resulting from significant increases in the mass and stiffness and the labor-intensive nature of the process have spurred researchers to explore alternative retrofitting techniques utilizing alternative materials. This drive towards innovation aims to overcome the drawbacks associated with conventional

RC jacketing while still effectively enhancing the structural integrity and performance of existing RC members [10–12].

Another vulnerability of RC structures erected under outdated regulations is their susceptibility to morphological issues stemming from a lack of seismic design awareness [13]. The construction of short structural elements introduces risks to the seismic response of the structure. Short elements, such as short columns and deep beams, are prone to exhibiting brittle failure modes, thereby reducing their contribution to the overall ductility of the structure [14]. Deep beams, mainly, are critical structural elements in RC structures due to their strong shear behavior [15].

In general, shear failure in RC structures can result in sudden and unexpected collapses of sections or even the entire structure, thereby jeopardizing the integrity and safety of occupants [16]. These structural deficiencies underscore the urgent need for retrofitting and strengthening measures to enhance the seismic resilience of existing RC structures and mitigate the associated risks posed by shear-induced failures.

A beam is categorized as deep or short based on its shear ratio, which is determined using Equation (1). Specifically, if the shear ratio, as computed by Equation (1), falls below 2.5, the beam is classified as deep. This classification is crucial in structural engineering, as it helps identify beams with distinctive shear behavior, informing design considerations and retrofitting strategies to ensure structural integrity and safety.

$$\alpha_s = \frac{\alpha_v}{d} = \frac{M}{V\,d} \leq 2.5 \tag{1}$$

where α_v represents the shear span of the element, d signifies the static height, and M and V denote the bending moment and shear force magnitudes of the cross-section, respectively. According to Saint-Venant's principle, the application of external load induces disturbed regions within deep beams, wherein the supports overlap, thus nullifying the areas where Bernoulli's principle applies to the beam in bending. Consequently, the analysis of deep beams necessitates adopting strut and tie simulation techniques, whereby concrete assumes the responsibility of transferring compressive forces while longitudinal reinforcement addresses tensile forces.

The mechanical response of deep beams is intricately influenced by their geometric properties, loading conditions, and the presence of transverse reinforcement. In RC structures, deep beams pose a pressing need for strengthening interventions due to their limited ductility and inadequate provision of transverse reinforcement.

The inability to extensively rehabilitate existing infrastructure and structures has spurred the development of novel monitoring and strengthening methodologies. These innovative approaches seek to address existing RC structures' deficiencies while enhancing their resilience and longevity in the face of dynamic loading and environmental challenges.

2. Proposed Innovation and Aim of the Study

In recent decades, fiber-reinforced polymers (FRPs) bonded externally with epoxy resins have emerged as go-to solutions for rehabilitating [17–19], reinforcing, upgrading, and repairing reinforced concrete (RC) structures. These applications span various structural elements [20], including shear-reinforced beams [21,22], torsion-reinforced beams [23], and shear-reinforced beam-column sub-assemblages [24], owing to their myriad advantages. These advantages include high tensile and fatigue strength, lightweight properties, and exceptional corrosion resistance [25,26]. Notably, carbon fiber-reinforced polymers (CFRPs) stand out for their superior performance in these properties compared to other FRPs.

Moreover, CFRPs boast high stiffness, enabling them to meet concrete structures' reinforcement demands while accommodating structural elements' deformation [27]. This feature enhances their suitability for retrofitting applications where maintaining structural integrity under varying loading conditions is paramount.

However, despite the numerous benefits offered by FRP materials, concerns surrounding their application in real structural settings exist. Issues such as premature delamination

failure and low fire resistance have been raised, prompting careful consideration during their implementation [28]. The reduced cohesion observed in the interfacial zone between the FRP composite and the concrete surface can lead to a lower-than-designed strain response, consequently diminishing the retrofitting efficiency of applied FRPs due to premature debonding [29,30].

Addressing these concerns and optimizing the performance of FRP materials in structural applications remain critical areas of research and development. By enhancing interfacial bond strength, improving fire resistance properties, and exploring innovative retrofitting techniques, the full potential of FRPs in enhancing the durability and resilience of RC structures can be achieved.

Furthermore, extensive research in the existing literature has consistently identified the predominant mode of failure in retrofitted RC elements using externally epoxy-bonded FRP composites as premature debonding or delamination of the FRP layer from the concrete substrate. This failure mode is typically induced by high-stress concentrations and is associated with brittle failure [31]. This phenomenon is particularly prevalent in T-shaped RC elements subjected to U-shaped strengthening schemes, where the presence of the slab restricts the applicability of FRP wrapping around the cross section and limits accessibility for the proper implementation of the end anchorage, thus exacerbating the risk of premature debonding failure.

In this context, Chalioris et al. investigated the potential benefits of a novel strengthening technique to enhance the shear capacity and improve the ductility of shear-critical RC deep beams [27]. The study focused on transverse reinforcement using solely C-FRP ropes. Two different configurations were explored for implementing C-FRP ropes: Embedded Through Section (ETS) for rectangular cross-sectioned beams and Near Surface Mounted (NSM) for T-shaped flanged deep beams. In both cases, the experimental performance of the applied shear strengthening technique yielded promising results, as the shear-critical beams under examination ultimately experienced flexural failure. These findings highlight the efficacy of the proposed strengthening approach in enhancing the structural performance of RC deep beams and mitigating the risk of shear-induced failure.

Hence, using C-FRP ropes to bolster the shear strength of RC structural elements emerges as a promising reinforcement technique. The versatility in anchoring arrangements for these ropes enables the full exploitation of their high tensile strength, providing flexibility in retrofitting design strategies. Furthermore, C-FRP ropes can be deployed in multiple configurations, including within pre-grooved notches along the height of the beam (NSM) [32,33] or embedded through the beam's web (ETS). This adaptability allows engineers to tailor the reinforcement approach to suit the specific requirements and constraints of each structural element, thereby maximizing the effectiveness of the strengthening intervention.

While the proposed techniques present potential advantages, significant shortcomings necessitate further exploration. Previous research has predominantly concentrated on early damage detection in epoxy-bonded FRP reinforcement, proposing non-destructive testing (NDT) methodologies, particularly in reinforcing RC structures with FRP composite materials. However, many of these methods prove impractical for large and complex structures, due to the structural limitations and the need for prior knowledge of the damage location. Moreover, most NDT approaches are characterized by time-consuming procedures, high costs, on-site access requirements, and a lack of continuous real-time monitoring capabilities. These limitations underscore the need for more robust and versatile techniques to effectively address structural monitoring and damage detection challenges [16].

As highlighted above, ensuring the seamless integration of existing structural elements with reinforcing materials presents a multifaceted challenge fraught with uncertainties. Consequently, monitoring the structural integrity of retrofitted structural elements is deemed beneficial for safely extending their service life. Numerous researchers have delved into the realm of Structural Health Monitoring (SHM) techniques applicable to concrete elements [34–36]. However, investigations specifically targeting the SHM of fiber-reinforced

concrete incorporating dispersed synthetic macrofibers [37,38], FRP composites [39–41], and studies focusing on C-FRP-reinforced structural elements are relatively scarce in the literature [42–45].

While the importance of SHM in enhancing the durability and safety of concrete structures is widely recognized, there remains a notable gap in research concerning the application of these techniques to fiber-reinforced concrete and FRP-reinforced elements. Addressing this gap through comprehensive investigations into SHM methodologies tailored to these materials holds great potential for advancing the field of structural monitoring and ensuring the long-term performance of retrofitted structures.

The experimental phase of this study involved the implementation of a novel monitoring system on a shear-strengthened beam subjected to four-point bending loading, aiming to assess and evaluate the effectiveness of the C-FRP rope strengthening technique. The proposed SHM method employed an Electro-Mechanical Impedance (EMI)-based system enabled with Piezoelectric Lead Zirconate-Titanate (PZT) sensors for wireless impedance monitoring (WiAMS) [46].

In this experimental setup, the voltage frequency responses of the PZT patches positioned along the perimeter of the C-FRP rope were recorded under varying levels of applied loading. These loading conditions corresponded to different structural health states or damage conditions. Additionally, efforts were made to quantitatively evaluate the contribution of the C-FRP ropes to the shear resistance of the RC beam. This evaluation was facilitated by analyzing statistical damage index values derived from the monitoring data. By correlating the response of the monitoring system with the applied loading and structural health conditions, valuable insights into the performance and effectiveness of the C-FRP rope strengthening technique were gleaned.

In the framework of this experimental study, the primary aim was to assess the feasibility of EMI as an applied SHM method for monitoring the structural integrity, efficacy, and performance of C-FRP ropes utilized as a retrofitting technique in a deep rectangular beam. Piezoelectric sensors were embedded alongside the ropes during installation to achieve this objective. The voltage responses of these PZTs in the frequency domain were then captured at various states of the applied loading and corresponding structural health conditions (loading levels).

Furthermore, an evaluation of the performance of the retrofitting technique was conducted at the examined loading levels. This evaluation was carried out using values derived from the Root Mean Square Deviation (RMSD), a commonly utilized statistical damage index. A unique aspect of this study involves the establishment of a combined methodology, which incorporates the responses of PZT patches embedded within the C-FRP ropes during pullout testing as baseline homogenizing data. By integrating data from both the experimental setup and the pullout testing, a comprehensive assessment of the C-FRP rope's performance under various loading conditions was achieved.

3. Experimental Program

3.1. Characteristics of the Deep Beam

The R-Deep Beam possessed a rectangular cross section along its length, measuring L = 1.6 m, with a width of b = 150 mm and a height of h = 300 mm. The longitudinal reinforcement of the R-Deep Beam was symmetrically arranged, comprising 2Ø14 bars placed in both the compression and tension zones. Additionally, stirrups of Ø8/50 were positioned only at the ends of the R-Deep Beam, near the supports, to secure the longitudinal reinforcement and prevent concrete spalling.

The shear span of the beam was α = 400 mm, and the total concrete cover was 35 mm, resulting in an effective depth of 265 mm. Consequently, the shear ratio α/d was calculated to be 1.51. A single-link C-FRP rope was vertically installed on the right shear span, while on the left shear span, the rope was inserted into a drilled hole at an inclination of approximately 52°. Both ropes were installed as ETS reinforcement. All the details of the beam are illustrated in Figure 1.

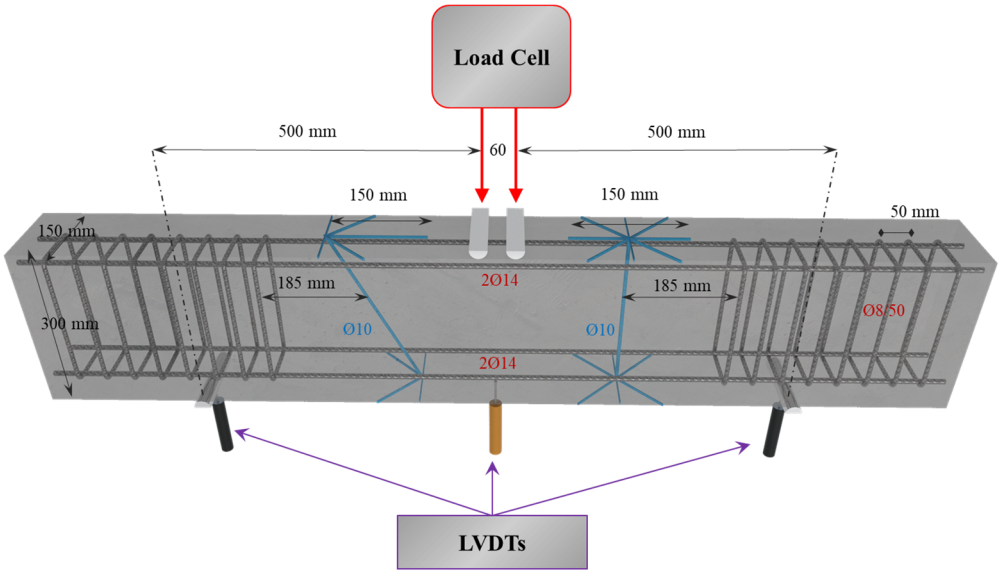

Figure 1. Geometry and reinforcement details of the beam R-Deep Beam.

The installation of ETS process for the C-FRP Ropes in "R-FRP" was as follows:

- Formation of the anchorage's tassels and drilling of the holes to the beam's web.
- Use of compressed air and a particular tool brush to remove the trapped dust inside the drilled holes.
- Epoxy resin impregnation of the rope following the manufacturer's technical data sheet.
- Epoxy resin filling of the anchorage's tassel grooves.
- C-FRP ropes and attached PZT-bonded insertion into the drilled holes.
- Filling of holes with epoxy resin to eliminate voids and enhance coherence among the embedded materials.
- Application of slight tension to the end of the ropes to achieve the final anchorage formation.
- Addition of more epoxy resin to the surface of the beams to achieve smoother grooves.

3.2. Materials

The study utilized C-FRP rope fabricated from unidirectional flexible carbon fibers. The specifications provided by the manufacturer included a cross-sectional area of approximately 28 mm^2, a minimum elongation before breaking of 1.6%, and a stiffness (modulus of elasticity) of 240 GPa for the unimpregnated fibers.

Subsequently, the rope underwent saturation with epoxy resin (Sikadur-52, SIKA Hellas Kryoneri, Greece), with the properties outlined in Table 1. This process aimed to enhance the mechanical properties and durability of the C-FRP rope. Additionally, epoxy paste (Sikadur-330, SIKA Hellas, Kryoneri, Greece) was employed to fill and seal the grooves drilled for the experimental setup, ensuring proper adhesion and structural integrity.

For assessing the mechanical properties of the concrete, standard concrete cylinders with dimensions of 150 mm in diameter and 300 mm in height were subjected to compression and splitting strength tests. On the day of testing, the concrete beams' average compressive and tensile strengths were measured to be 28.0 MPa and 2.70 MPa, respectively. The concrete mix utilized in the experiments contained maximum aggregate particles with a diameter of 16 mm.

The deformed steel rebars (∅14 mm) had a yield strength of 580 MPa, while the mild steel stirrups (∅8 mm) had a yield strength of 310 MPa.

Table 1. Mechanical properties of C-FRP ropes.

Material	Mechanical Properties	
C-FRP rope SikaWrap FX-50C (Laminate)	Tensile strength (TS) Elastic modulus in tension Elongation at break in tension	2100 GPa 230 GPa 0.87%
Sikadur 300	TS Elastic modulus in tension	45 MPa 3.5 GPa
Sikadur 330	TS Elastic modulus in tension	30 MPa 4.5 GPa
Sika Anchorfix 3+	Compressive strength	114 MPa

3.3. Test Setup

The beam underwent testing utilizing a four-point bending setup, as illustrated in Figure 2. A hydraulic actuator, controlled by a servo-controlled machine, applied a gradually increasing load (monotonic force) to the upper surface of the beams through two evenly spaced steel rollers positioned 60 mm apart. The beam was supported on its edges by two steel roller supports on each side. A load cell, boasting high precision with an accuracy of 0.05 kN, measured the applied force with utmost accuracy.

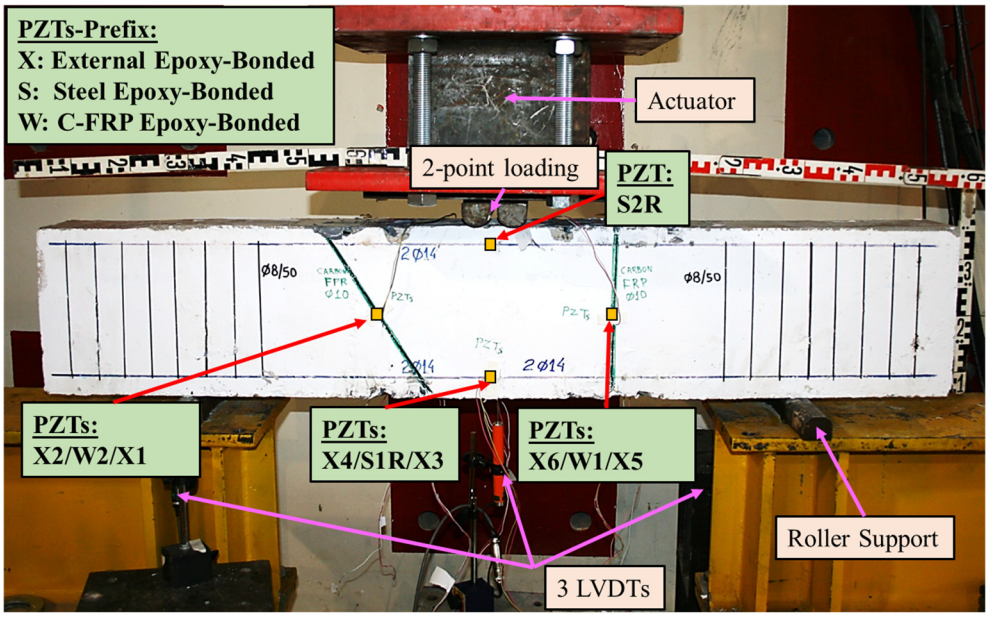

Figure 2. Test setup, instrumentation, and PZTs' configuration.

In addition to the load measurement, three sensors, specifically linear variable differential transducers (LVDTs), were employed to measure the deflections of the beams.

3.4. Electro-Mechanical Impedance (EMI) Technique

The EMI technique utilizes PZT transducers, leveraging the advantageous properties of the piezoelectric phenomenon. When subjected to mechanical stress, PZT transducers generate a superficial electric charge, and conversely, applying an electric field induces mechanical vibration. Thus, by harnessing this phenomenon, the EMI activates and induces vibrations in bonded or embedded PZT transducers within a host structure. Any change in the structure's mechanical impedance (or inverse admittance) is mirrored in alterations to the extracted electrical signal from the PZT (either in voltage or frequency response). The interaction between the PZT and the host structure is represented as an admittance signature comprising a real-part (conductance) and an imaginary part (sus-

ceptance). These interactions manifest structural characteristics within the signature, as described by Equation (2) for the complex admittance, $\overline{Y}$, of the affixed PZT patch:

$$\overline{Y} = \frac{\overline{I}}{\overline{V}} = G + Bj = 4\omega j \frac{L^2}{h}\left[\overline{\varepsilon_{33}^T} - \frac{2d_{31}^2\overline{Y^E}}{(1-\nu)} + \frac{2d_{31}^2\overline{Y^E}}{(1-\nu)}\left(\frac{Z_{a,eff}}{Z_{s,eff}+Z_{a,eff}}\right)\left(\frac{tankL}{kL}\right)\right] \quad (2)$$

where $\overline{V}$: harmonic alternating voltage supplied to the circuit, $\overline{I}$: current passing through PZT, G: conductance (the real part of admittance), B: susceptance (the imaginary part of admittance), j: imaginary unit, v: angular frequency, L: half-length of the patch, h: thickness of the patch, d_{31}: piezoelectric strain coefficient of the PZT, $Z_{a,eff}$: short-circuited effective mechanical impedance, $Z_{s,eff}$: effective structural impedance, n: Poisson's ratio, k: wave number related to the angular frequency, Y^E: complex Young's modulus of elasticity under constant electric field, and $\overline{\varepsilon_{33}^T}$: complex electric permittivity of PZT patch along the axis at constant stress.

Any changes in the RC beam, such as alterations in its mass and stiffness properties, will inevitably result in modifications to the structural parameters, consequently affecting the effective structural impedance. These alterations will also lead to modifications in the admittance $\overline{Y}$, as defined by Equation (2), thereby indicating the health status of the element.

In this experimental study, the selected approach for detecting changes in the installed C-FRP ropes involved the utilization of PZT transducers excited by a sinusoidal harmonic voltage of 2.5 V within a specific frequency range spanning from 10 to 250 kHz, with increments of 1 kHz per step. Serving as both actuators and sensors, the PZT transducers generated the voltage signal and captured the EMI signatures, which were then processed through a custom-designed wireless device known as WiAMS [40,46]. This device is equipped with high processing power, allowing for rapid and extensive calculations, and can be operated remotely, as depicted in Figure 3.

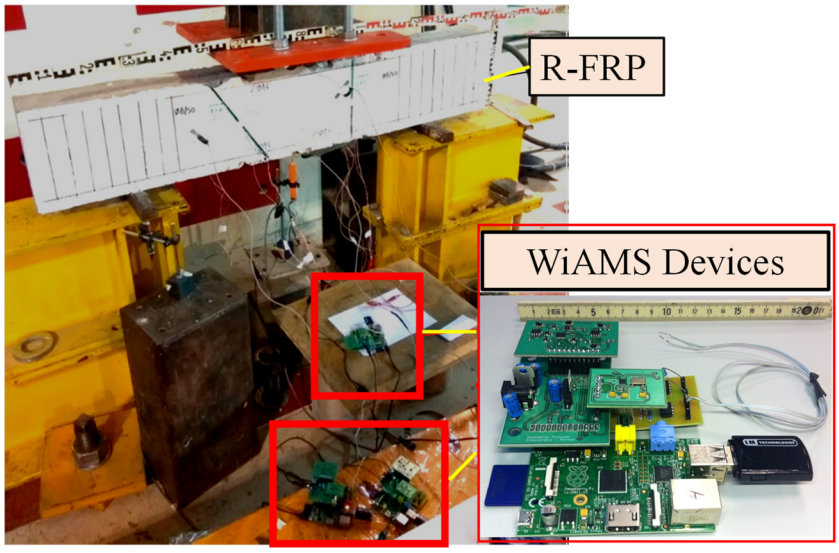

Figure 3. WiAMS devices of the proposed SHM method.

At the outset, EMI measurements were carried out on the beam in its initial pristine state, establishing a baseline for its declared healthy condition. Subsequently, these measurements were repeated under various potential damage scenarios, simulating conditions that could compromise the structural integrity. The obtained results were then meticulously compared to evaluate any deviations using statistical metrics, particularly the Root Mean Square Deviation (RMSD). This comparative analysis enabled the detection and assessment of structural changes, providing valuable insights into the beam's health status and integrity under different loading conditions. At this point, it is noteworthy to mention that

all the voltage measurements were conducted in controlled laboratory conditions to avoid interferences due to temperature and humidity fluctuations.

3.5. PZT Patches' Installation

The beam R-FRP was equipped with identical small and thin PZT transducers, each measuring 10 × 10 × 2 mm. These PZT patches, designated as PIC151, were manufactured by the PI Ceramics company. A total of ten PZTs were strategically positioned within the beam in various configurations, as illustrated in Figure 2. Six PZTs (three placed in the front and three in the rear) were externally epoxy-bonded to critical mechanical locations on the concrete surface, particularly at locations prone to flexural and shear diagonal cracks, denoted as "X1–X6". Two additional PZTs were bonded to the steel reinforcement, with one positioned in the middle of the tensional reinforcing bar (S2R) and the other in the middle of the flexural reinforcing bar (S1R).

The remaining two PZT patches were meticulously placed on the C-FRP ropes according to the following procedure: The PZT patches were simultaneously embedded with the ropes inserted into each drilled hole. Each PZT patch was securely affixed to the rope using an epoxy adhesive, and the welded wires were carefully tied to the rope using a tire-up component and a steel wire to ensure the final designed position of the PZT patch inside the hole. The tying position was strategically selected so that the PZT patch ended up bonded internally to the drilled hole at the midpoint of the rope's traversing length. A steel wire served as an assisting tool for guiding the rope, PZT patch, and wires through the hole, after which it was removed. These two patches were designated as W1 and W2, respectively, as depicted in Figure 4.

Figure 4. Insertion of the PZT transducers in the drilled holes assembled with the C-FRP ropes.

4. Results and Discussion

4.1. Pullout Test

To assess the effectiveness of the EMI-based SHM system in evaluating bond strength, a pullout test was conducted using a straight configuration for anchoring the C-FRP ropes, without any protruding end. In this regard, cubic concrete specimens were fabricated to serve as hosts for the anchorage, as illustrated in Figure 5.

The process involved impregnating the C-FRP ropes with a suitable resin and then inserting them into pre-drilled holes within the cube specimens. The anchoring resin was applied to infill the holes to ensure optimal bonding conditions between the rope and the concrete. Detailed dimensions of the cube specimens, including the length of the embedded section and the anchor configuration, are presented in Figure 5. This setup provided a controlled environment for evaluating the bond strength between the C-FRP ropes and

the concrete substrate, facilitating an accurate assessment of the effectiveness of the SHM system in detecting potential bond defects or degradation over time.

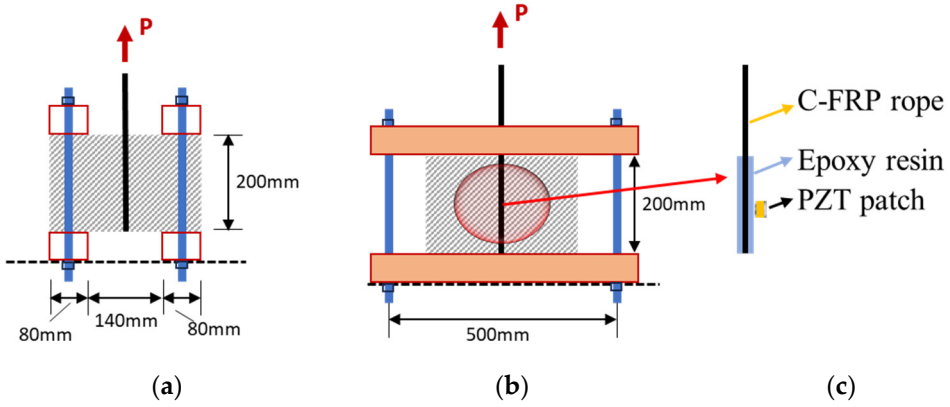

Figure 5. (**a**,**b**) Pullout testing configuration; (**c**) details of the embedded PZTs transducers on C-FRP ropes.

The setup underwent a direct pullout test, applying monotonic loading at a constant displacement rate of 0.5 mm/min until reaching failure. During the test, three laser sensors positioned atop the protruding end of the rope meticulously recorded the extent of free end slip, as depicted in Figure 6a. Additionally, a comprehensive data system acquired the applied loading and the corresponding free end slip measurements.

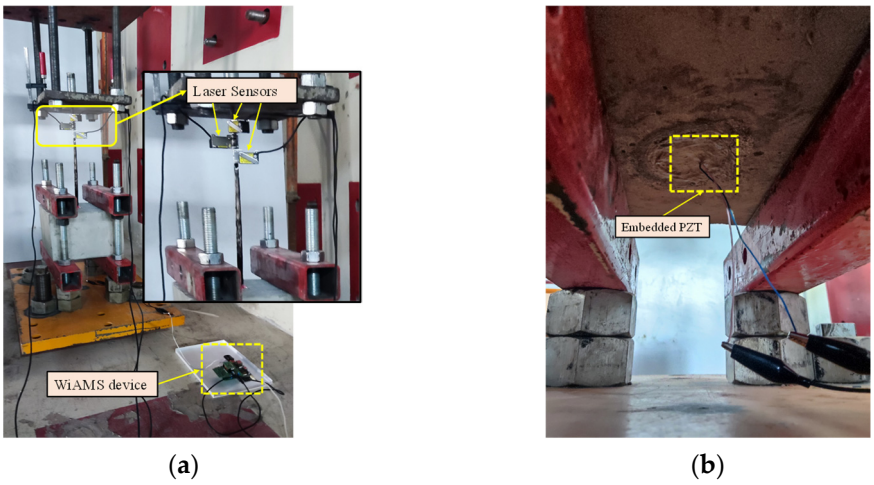

Figure 6. (**a**) Pullout testing configuration and WiAMS device; (**b**) upside-down view of the embedded PZT transducers on the C-FRP ropes' configuration.

Furthermore, a strategically positioned PZT patch was bonded onto the rope within the pre-drilled hole of the cube, as illustrated in Figure 6b. This PZT patch played a crucial role in monitoring and capturing the structural response of the anchorage system, providing valuable insights into the bond behavior between the C-FRP rope and the concrete substrate throughout the pullout test.

The voltage–frequency diagram corresponding to the pullout test is depicted in Figure 7. In a black continuous line, the response at the pristine condition of the C-FRP rope is depicted and is notated as "Healthy". Further, in cyan and blue continuous lines, the voltage response measurements at the ascending stage and peak tensile strength are depicted and denoted as "Dam1" and "Dam2", respectively. Moreover, in the green continuous line, the voltage measurement at the descending post-peak stage is depicted and denoted as "Dam3". Upon scrutiny of the diagram, discernible deviations were observed in the response curves between the undamaged state and different levels of simulated damage

within the frequency range of 120–250 kHz. This observation underscores the sensors' ability to detect debonding conditions or the failure of the C-FRP ropes. The magnitude of the step change in the overall response of the PZT across the specified frequency range indicated the extent of failure. These deviations in the voltage–frequency diagram provide valuable insights into the structural integrity of the anchorage system and enable the identification of potential bond defects or degradation during the pullout test.

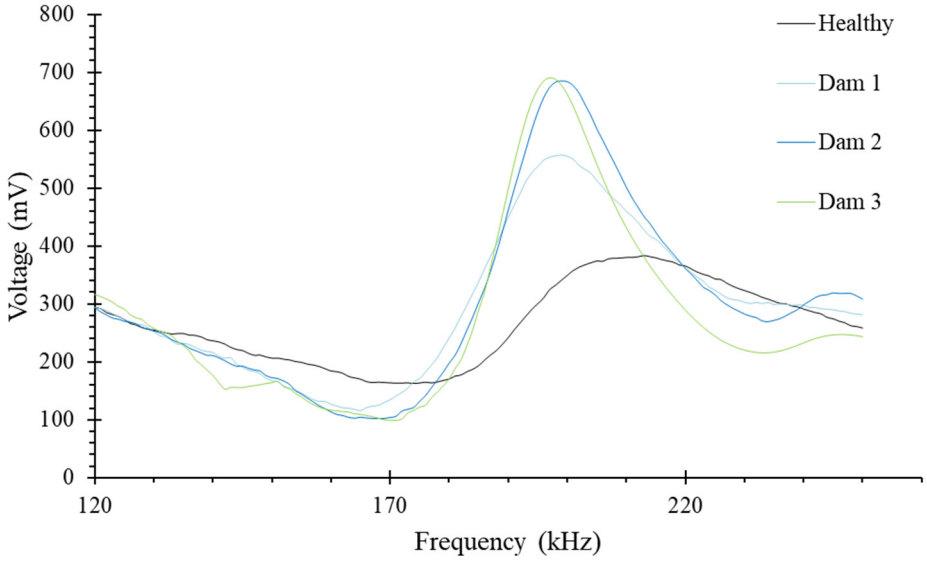

Figure 7. Voltage response of PZT under pullout testing of the C-FRP rope.

4.2. Deep Beam Loading Test

The comprehensive performance of the beam with a rectangular cross section, illustrated by the curves depicting applied load versus mid-span deflection, is presented in Figure 8. For a detailed analysis of the overall behavior of these beams, readers can refer to prior research conducted by Chalioris et al. [27]. Furthermore, the cracking pattern observed during the failure of the tested beams is also depicted in Figure 8, providing additional insights into the structural response under varying loading conditions.

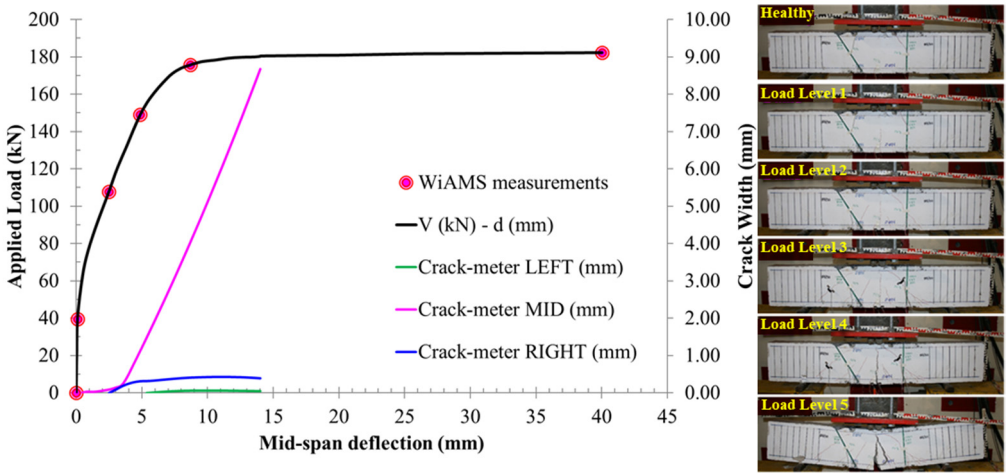

Figure 8. Cracking pattern and experimental behavior of the R-FRP specimen.

4.3. Data Analysis

Utilizing statistical analysis to elaborate on the EMI signatures can be a valuable tool for transforming variations in EMI signatures between the pristine condition and subsequent conditions into stress index metrics. Thus, the acquired voltage responses

were analyzed and evaluated within this context using the statistical index RMSD. The expression of the index is provided below in Equation (3).

$$RMSD = \sqrt{\frac{\sum_{r=1}^{M}\left(\left|V_p(f_r)\right|_D - \left|V_p(f_r)\right|_0\right)^2}{\sum_{r=1}^{M}\left(\left|V_p(f_r)\right|_0\right)^2}} \quad (3)$$

where $\left|V_p(f_r)\right|_0$ refers to the voltage response at the initial pristine state, while $\left|V_p(f_r)\right|_D$ refers to the voltage responses in any subsequent state.

4.4. Evaluation of the Efficacy of Retrofitting Technique

Based on the results obtained from the pullout test and the extracted RMSD index values at specific loading levels until the final fracture of the C-FRP rope (as shown in Figure 9), the evaluation of the residual shear strength bearing capacity was attempted. This evaluation was conducted through a homogenizing approach, which involved correlating the RMSD values of the pullout test with those acquired from the deep beam.

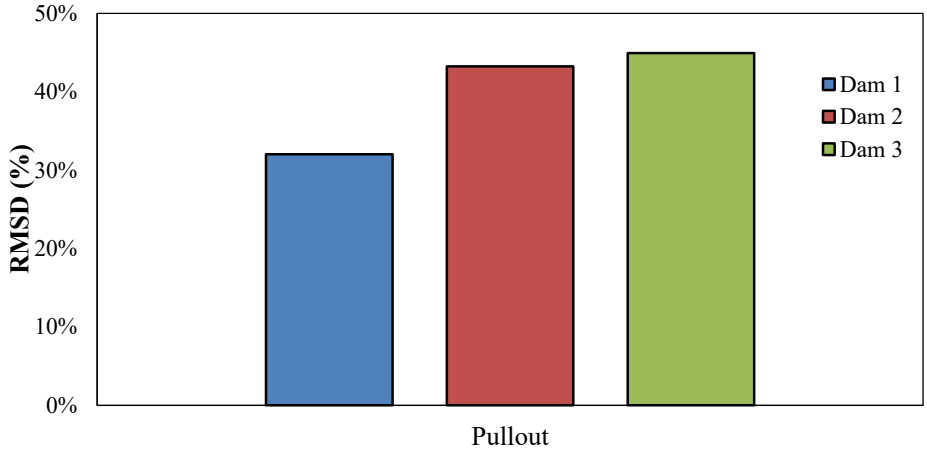

Figure 9. RMSD values of the PZT under pullout testing of the C-FRP rope.

The ultimate pullout load recorded was approximately 27 kN, corresponding to a 30 mm rope displacement at failure. Initially, the Root Mean Square Deviation (RMSD) index value at the failure state of the pullout test was standardized to a ratio of 100%, representing total failure. Conversely, the 100%-RMSD values at the point of loss of the rope's shear strength contribution were computed as 0%, as the final fracture and the complete loss of tensile strength are inherently interconnected. This alignment with the experimental condition, wherein the rope is cut into two pieces at failure, as depicted in Figure 10, further validates this approach.

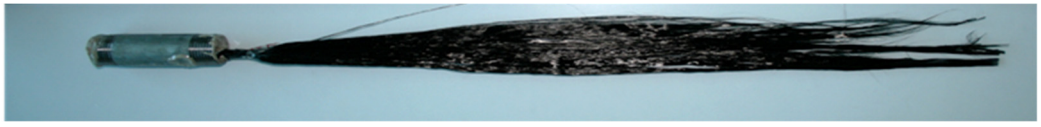

Figure 10. Final failure mode of the C-FRP rope.

Furthermore, all the RMSD index values obtained from the two bonded PZTs embedded within the through-section ropes were standardized relative to the values obtained from the pullout test. This homogenization process allowed for a direct comparison, and the residual shear strength of ropes W1 and W2, respectively, is illustrated in Figure 11. By aligning the RMSD index values from the PZT-enabled monitoring system with those obtained from the pullout test, valuable insights were gained into the ropes' residual shear strength and their performance under varying loading conditions.

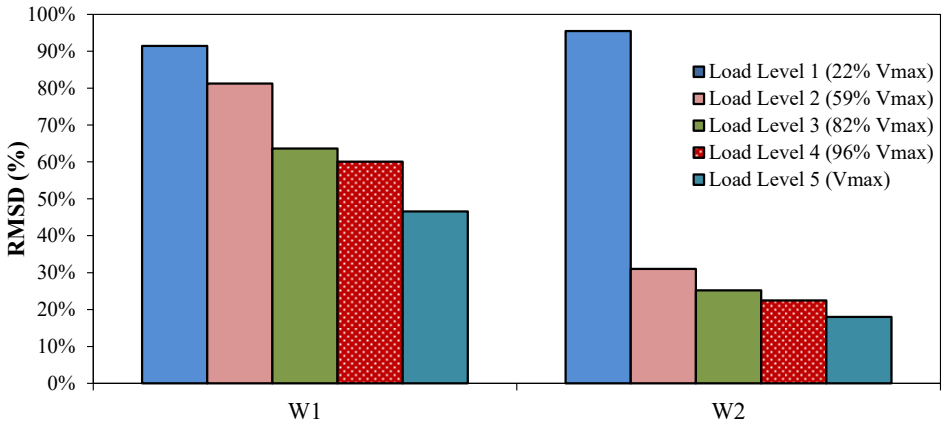

Figure 11. Residual shear strength capacity of the embedded C-FRP ropes.

In Figure 11, the gradual reduction in the shear strength capacity of the W1 rope can be observed, primarily attributed to the formation of the first shear crack in the right span. As the loading increased, this crack continued to widen, resulting in the concrete absorbing a significant portion of the developed shear stresses. Consequently, the contribution of the right rope diminished progressively. Conversely, the inclined positioning of rope W2 proved advantageous in limiting the development of cracking in the left shear span. This observation is corroborated by the cracking pattern depicted in Figure 8, where it is evident that the first left shear crack formed at loading level 4.

Furthermore, this is reflected in the left crack-meter values, where the crack opening was notably reduced compared to that in the right span. Thus, up to that loading level, the rope lost approximately 78% of its total estimated shear strength. These insights shed light on the dynamic interaction between the strengthening elements and the structural behavior, underscoring the importance of thoughtful positioning and design considerations in optimizing performance and resilience against shear-induced failure mechanisms.

To further assess the effectiveness of the innovative strengthening technique, the analytical model proposed by Mofidi et al. [47] was applied to compute the ropes' contribution to the beam's total shear strength at the failure state. Additionally, it is crucial to ensure that the effective strain of the C-FRP ropes does not exceed 0.4% to achieve sufficient interlock of concrete's aggregate and intercept crack opening, as recommended by ACI 440.2R-08 [48].

By implementing all the proposed calculations outlined in the relevant work of Chalioris et al. [27], the following values were derived:

$V_{f,ETS}$, R_{rope} = 39.6 kN

$V_{f,ETS}$, L_{rope} = 53.3 kN

Furthermore, based on the assumption that the mean laminate tensile strength of the rope was approximately 2000 N/mm^2, the total residual shear strength for rope W1 was calculated as $V_{f,ETS}$, R_{rope} = 31.8 kN. Similarly, for rope W2, the residual shear strength was computed as $V_{f,ETS}$, L_{rope} = 49.2 kN, demonstrating a remarkable proximity of 92.3% to the analytical calculated results. These findings underscore the effectiveness of the proposed strengthening technique and highlight its potential for accurately estimating the residual shear strength in real-scale applications.

5. Conclusions

In this experimental project, an investigation into the effectiveness of an innovative strengthening technique involving the use of C-FRP ropes as shear transverse reinforcement was conducted. This assessment was carried out by implementing an EMI-based method enabled by PZT sensors. Additionally, a modified application of the statistical index metric RMSD was employed to evaluate the efficacy of the strengthening technique.

Unlike conventional usage of the RMSD index to express damage levels or loading impacts, this study used the 100%-RMSD index values to depict the residual shear

strength capacity. This novel approach assessed the strengthening technique's performance, demonstrating promising convergence and precision with the analytical predictions. This comparative analysis enhances the understanding of the effectiveness of the strengthening technique and provides valuable data for further optimization and refinement of structural reinforcement strategies.

Moreover, the results obtained through the applied EMI-based method present a significant opportunity to serve as a reliable supplementary tool for diagnosing damage defects and evaluating the effectiveness of fiber-based materials in real-time scenarios. It is worth noting that the presence of epoxy resin within the drilled holes may slightly impact the precision of the experimental results obtained through the EMI-based PZT-enabled approach.

Furthermore, while this study shows promising alignment with analytical predictions regarding the contribution of the rope to shear strength, additional experimental work is warranted to evaluate further and enhance the fidelity of the proposed assessment methodology. By undertaking further experimentation, the aim is to ensure the robustness and reliability of this novel approach for real-scale applications, thereby advancing the field of structural strengthening techniques.

Author Contributions: Conceptualization, N.A.P., M.C.N. and G.M.S.; methodology, N.A.P. and M.C.N.; formal analysis, N.A.P. and G.M.S.; investigation, C.E.C., N.A.P. and G.M.S.; data curation, N.A.P. and M.C.N.; writing—original draft preparation, N.A.P. and M.C.N.; writing—review and editing, N.A.P. and C.E.C.; visualization, M.C.N.; supervision, C.E.C. All authors have read and agreed to the published version of the manuscript.

Funding: This research received no external funding.

Data Availability Statement: The original contributions presented in the study are included in the article, further inquiries can be directed to the corresponding author/s.

Conflicts of Interest: The authors declare no conflicts of interest.

References

1. Zhang, T.; Visintin, P.; Oehlers, D.J. Shear Strength of RC Beams with Steel Stirrups. *J. Struct. Eng.* **2016**, *142*, 04015135. [CrossRef]
2. Zararis, P.D. Shear Compression Failure in Reinforced Concrete Deep Beams. *J. Struct. Eng.* **2003**, *129*, 544–553. [CrossRef]
3. Godat, A.; L'Hady, A.; Chaallal, O.; Neale, K.W. Bond Behavior of the ETS FRP Bar Shear-Strengthening Method. *J. Compos. Constr.* **2012**, *16*, 529–539. [CrossRef]
4. Azam, R.; Soudki, K.; West, J.S.; Noël, M. Behavior of Shear-Critical RC Beams Strengthened with CFRCM. *J. Compos. Constr.* **2018**, *22*, 04017046. [CrossRef]
5. Karayannis, C.G.; Sirkelis, G.M. Strengthening and Rehabilitation of RC Beam–Column Joints Using Carbon-FRP Jacketing and Epoxy Resin Injection. *Earthq. Engng Struct. Dyn.* **2008**, *37*, 769–790. [CrossRef]
6. Karayannis, C.G.; Naoum, M.C. Torsional Behavior of Multistory RC Frame Structures Due to Asymmetric Seismic Interaction. *Eng. Struct.* **2018**, *163*, 93–111. [CrossRef]
7. Tsonos, A.G. Effectiveness of CFRP Jackets in Post-Earthquake and Pre-Earthquake Retrofitting of Beam-Column Subassemblages. *Struct. Eng. Mech.* **2007**, *27*, 393–408. [CrossRef]
8. Lampropoulos, A.P.; Dritsos, S.E. Modeling of RC Columns Strengthened with RC Jackets. *Earthq Engng Struct Dyn* **2011**, *40*, 1689–1705. [CrossRef]
9. Ma, C.-K.; Apandi, N.M.; Sofrie, C.S.Y.; Ng, J.H.; Lo, W.H.; Awang, A.Z.; Omar, W. Repair and Rehabilitation of Concrete Structures Using Confinement: A Review. *Constr. Build. Mater.* **2017**, *133*, 502–515. [CrossRef]
10. Azam, R.; Soudki, K.; West, J.S.; Noël, M. Strengthening of Shear-Critical RC Beams: Alternatives to Externally Bonded CFRP Sheets. *Constr. Build. Mater.* **2017**, *151*, 494–503. [CrossRef]
11. Ferreira, D.; Oller, E.; Marí, A.; Bairán, J. Numerical Analysis of Shear Critical RC Beams Strengthened in Shear with FRP Sheets. *J. Compos. Constr.* **2013**, *17*, 04013016. [CrossRef]
12. Baggio, D.; Soudki, K.; Noël, M. Strengthening of Shear Critical RC Beams with Various FRP Systems. *Constr. Build. Mater.* **2014**, *66*, 634–644. [CrossRef]
13. Aguilar, V. Shear Strength of Concrete Members: Challenges, Recent Developments and Possibilities. *Adv. Civ. Eng. Technol.* **2020**, *4*, 1–2. [CrossRef]
14. Işık, E.; Ulutaş, H.; Harirchian, E.; Avcil, F.; Aksoylu, C.; Arslan, M.H. Performance-Based Assessment of RC Building with Short Columns Due to the Different Design Principles. *Buildings* **2023**, *13*, 750. [CrossRef]

15. Pan, Z.; Li, B. Evaluation of Shear Strength Design Methodologies for Slender Shear-Critical RC Beams. *J. Struct. Eng.* **2013**, *139*, 619–622. [CrossRef]
16. Papadopoulos, N.A.; Naoum, M.C.; Sapidis, G.M.; Chalioris, C.E. Cracking and Fiber Debonding Identification of Concrete Deep Beams Reinforced with C-FRP Ropes against Shear Using a Real-Time Monitoring System. *Polymers* **2023**, *15*, 473. [CrossRef]
17. Bilotta, A.; Ceroni, F.; Di Ludovico, M.; Nigro, E.; Pecce, M.; Manfredi, G. Bond Efficiency of EBR and NSM FRP Systems for Strengthening Concrete Members. *J. Compos. Constr.* **2011**, *15*, 757–772. [CrossRef]
18. Seo, S.-Y.; Feo, L.; Hui, D. Bond Strength of near Surface-Mounted FRP Plate for Retrofit of Concrete Structures. *Compos. Struct.* **2013**, *95*, 719–727. [CrossRef]
19. Breveglieri, M.; Aprile, A.; Barros, J.A.O. Embedded Through-Section Shear Strengthening Technique Using Steel and CFRP Bars in RC Beams of Different Percentage of Existing Stirrups. *Compos. Struct.* **2015**, *126*, 101–113. [CrossRef]
20. Li, P.; Wang, H.; Nie, D.; Wang, D.; Wang, C. A method to analyze the long-term durability performance of underground reinforced concrete culvert structures under coupled mechanical and environmental loads. *J. Intell. Constr.* **2023**, *1*, 9180011. [CrossRef]
21. Said, M.; Adam, M.A.; Mahmoud, A.A.; Shanour, A.S. Experimental and Analytical Shear Evaluation of Concrete Beams Reinforced with Glass Fiber Reinforced Polymers Bars. *Constr. Build. Mater.* **2016**, *102*, 574–591. [CrossRef]
22. Naoum, M.; Sapidis, G.; Papadopoulos, N.; Golias, E.; Chalioris, C. Structural Health Monitoring of Reinforced Concrete Beam-Column Joints Using Piezoelectric Transducers. In Proceedings of the International RILEM Conference on Synergising Expertise towards Sustainability and Robustness of Cement-Based Materials and Concrete Structures, Milos, Greece, 14–16 June 2023; Jędrzejewska, A., Kanavaris, F., Azenha, M., Benboudjema, F., Schlicke, D., Eds.; RILEM Bookseries. Springer Nature: Cham, Switzerland, 2023; Volume 43, pp. 945–956. [CrossRef]
23. Turner, L.; Davies, V.C. Plain and reinforced concrete in torsion, with particular reference to reinforced-concrete beams. *Sel. Eng. Pap.* **1934**, *1*, 165. [CrossRef]
24. Chalioris, C.E.; Papadopoulos, N.A.; Sapidis, G.; Naoum, M.C.; Golias, E. EMA-Based Monitoring Method of Strengthened Beam-Column Joints. In Proceedings of the International ISCRAM Conference, Omaha, NE, USA, 28–31 May 2023; pp. 853–873. [CrossRef]
25. Alam, P.; Mamalis, D.; Robert, C.; Floreani, C.; Brádaigh, C.M.Ó. The Fatigue of Carbon Fibre Reinforced Plastics—A Review. *Compos. Part B Eng.* **2019**, *166*, 555–579. [CrossRef]
26. Zhu, X.; Abe, H.; Hayashi, D.; Tanaka, H. Behavioral characteristics of RC beams with non-uniform corrosion along the reinforcement. *J. Intell. Constr.* **2023**, *1*, 9180019. [CrossRef]
27. Chalioris, C.; Kosmidou, P.-M.; Papadopoulos, N. Investigation of a New Strengthening Technique for RC Deep Beams Using Carbon FRP Ropes as Transverse Reinforcements. *Fibers* **2018**, *6*, 52. [CrossRef]
28. Bazli, M.; Abolfazli, M. Mechanical Properties of Fibre Reinforced Polymers under Elevated Temperatures: An Overview. *Polymers* **2020**, *12*, 2600. [CrossRef]
29. Kytinou, V.K.; Gribniak, V.; Zapris, A.G.; Chalioris, C.E. An Innovative Health-Monitoring Approach for Fiber-Reinforced Polymer Debonding Diagnosis Through Pullout and Shear Tests. In *Analytical and Experimental Methods in Mechanical and Civil Engineering*; Springer: Cham, Switzerland, 2024; Volume 28, pp. 228–239. [CrossRef]
30. Ju, S.; Li, D.; Jia, J. Experimental Investigation and Damage Evaluation of a Novel Bond Type Anchorage for Carbon Fiber Reinforced Polymer Tendons. *J. Civ. Struct. Health Monit.* **2023**, *13*, 117–132. [CrossRef]
31. El-Sisi, A.A.; El-Emam, H.M.; El-Kholy, A.E.-M.I.; Ahmad, S.S.; Sallam, H.M.; Salim, H.A. Structural Behavior of RC Beams Containing Unreinforced Drilled Openings with and without CFRP Strengthening. *Polymers* **2022**, *14*, 2034. [CrossRef]
32. Baena, M.; Jahani, Y.; Torres, L.; Barris, C.; Perera, R. Flexural Performance and End Debonding Prediction of NSM Carbon FRP-Strengthened Reinforced Concrete Beams under Different Service Temperatures. *Polymers* **2023**, *15*, 851. [CrossRef]
33. Perera, R.; Gil, A.; Torres, L.; Barris, C. Diagnosis of NSM FRP Reinforcement in Concrete by Using Mixed-Effects Models and EMI Approaches. *Compos. Struct.* **2021**, *273*, 114322. [CrossRef]
34. Pellone, L.; Ciminello, M.; Mercurio, U.; Apuleo, G.; Concilio, A. A Structural Health Monitoring System for Bond Line Flaws Detection on a Full-Scale Wingbox Section Demonstrator. *Appl. Mech.* **2024**, *5*, 36–57. [CrossRef]
35. Ai, D.; Mo, F.; Yang, F.; Zhu, H. Electromechanical Impedance-Based Concrete Structural Damage Detection Using Principal Component Analysis Incorporated with Neural Network. *J. Intell. Mater. Syst. Struct.* **2022**, *33*, 2241–2256. [CrossRef]
36. Ai, D.; Zhang, D.; Zhu, H. Damage Localization on Reinforced Concrete Slab Structure Using Electromechanical Impedance Technique and Probability-Weighted Imaging Algorithm. *Constr. Build. Mater.* **2024**, *424*, 135824. [CrossRef]
37. Sapidis, G.M.; Kansizoglou, I.; Naoum, M.C.; Papadopoulos, N.A.; Chalioris, C.E. A Deep Learning Approach for Autonomous Compression Damage Identification in Fiber-Reinforced Concrete Using Piezoelectric Lead Zirconate Titanate Transducers. *Sensors* **2024**, *24*, 386. [CrossRef]
38. Wang, Z.; Chen, D.; Zheng, L.; Huo, L.; Song, G. Influence of Axial Load on Electromechanical Impedance (EMI) of Embedded Piezoceramic Transducers in Steel Fiber Concrete. *Sensors* **2018**, *18*, 1782. [CrossRef]
39. Naoum, M.C.; Papadopoulos, N.A.; Voutetaki, M.E.; Chalioris, C.E. Structural Health Monitoring of Fiber-Reinforced Concrete Prisms with Polyolefin Macro-Fibers Using a Piezoelectric Materials Network under Various Load-Induced Stress. *Buildings* **2023**, *13*, 2465. [CrossRef]

40. Naoum, M.C.; Sapidis, G.M.; Papadopoulos, N.A.; Voutetaki, M.E. An Electromechanical Impedance-Based Application of Real-time Monitoring for the Load-Induced Flexural Stress and Damage in Fiber-Reinforced Concrete. *Fibers* **2023**, *11*, 34. [CrossRef]
41. Khatir, A.; Capozucca, R.; Kathir, S.; Magagnini, E.; Benaissa, B.; Cuong-Le, T. An efficient improved gradient boosting for strain prediction in NSM FRP strengthened RC beam. *Front. Struct. Civ. Eng.* 2024, *in press*.
42. Reddy, P.N.; Kavyateja, B.V.; Jindal, B.B. Structural Health Monitoring Methods, Dispersion of Fibers, Micro and Macro Structural Properties, Sensing, and Mechanical Properties of Self-sensing Concrete—A Review. *Struct. Concr.* **2021**, *22*, 793–805. [CrossRef]
43. Perera, R.; Huerta, M.C.; Baena, M.; Barris, C. Analysis of FRP-Strengthened Reinforced Concrete Beams Using Electromechanical Impedance Technique and Digital Image Correlation System. *Sensors* **2023**, *23*, 8933. [CrossRef]
44. Li, D.; Zhou, J.; Ou, J. Damage, Nondestructive Evaluation and Rehabilitation of FRP Composite-RC Structure: A Review. *Constr. Build. Mater.* **2021**, *271*, 121551. [CrossRef]
45. Khatir, A.; Capozucca, R.; Khatir, S.; Magagnini, E.; Benaissa, B.; Le Thanh, C.; Wahab, M.A. A new hybrid PSO-YUKI for double cracks identification in CFRP cantilever beam. *Compos. Struct.* **2023**, *311*, 116803. [CrossRef]
46. Providakis, C.; Tsistrakis, S.; Voutetaki, M.; Tsompanakis, J.; Stavroulaki, M.; Agadakos, J.; Kampianakis, E.; Pentes, G.; Liarakos, E. An Innovative Active Sensing Platform for Wireless Damage Monitoring of Concrete Structures. *Curr. Smart Mater.* **2016**, *1*, 49–62. [CrossRef]
47. Mofidi, A.; Chaallal, O.; Benmokrane, B.; Neale, K. Experimental Tests and Design Model for RC Beams Strengthened in Shear Using the Embedded Through-Section FRP Method. *J. Compos. Constr.* **2012**, *16*, 540–550. [CrossRef]
48. ACI (American Concrete Institute). *Guide for the Design and Construction of Externally Bonded FRP Systems for Strengthening Concrete Structures*; ACI-440.2R-08; American Concrete Institute (ACI): Farmington Hills, MI, USA, 2008; p. 76.

Disclaimer/Publisher's Note: The statements, opinions and data contained in all publications are solely those of the individual author(s) and contributor(s) and not of MDPI and/or the editor(s). MDPI and/or the editor(s) disclaim responsibility for any injury to people or property resulting from any ideas, methods, instructions or products referred to in the content.